Am J Transl Res 2025;17(11):8463-8480
www.ajtr.org /ISSN:1943-8141/AJTR0166643

Original Article

Exploring the potential of Buzhong Yiqi decoction in the treatment of membranous nephropathy: a comprehensive study combining bioinformatics, network pharmacology, and experimental validation

Yihan Wang[1,2*], Ruizhi Tan[2*], Qi Liu[3], Jian Jia[2], Junming Fan[1,4], Li Wang[2]

[1]Department of Nephrology, The Affiliated Traditional Chinese Medicine Hospital, Southwest Medical University, Luzhou 646000, Sichuan, China; [2]Research Center of Integrated Traditional Chinese and Western Medicine, The Affiliated Traditional Chinese Medicine Hospital, Southwest Medical University, Luzhou 646000, Sichuan, China; [3]Department of Neurosurgery, The Affiliated Traditional Chinese Medicine Hospital, Southwest Medical University, Luzhou 646000, Sichuan, China; [4]Department of Nephrology, The First Affiliated Hospital of Chengdu Medical College, Chengdu 610500, Sichuan, China. [*]Equal contributors.

Received June 8, 2025; Accepted October 23, 2025; Epub November 15, 2025; Published November 30, 2025

Abstract: Background and Objective: Buzhong Yiqi Decoction (BZYQ), a classic Chinese herbal formula, demonstrates clinical efficacy in treating membranous nephropathy (MN), yet its molecular mechanisms remains undefined. This study aims to uncover the therapeutic mechanisms of BZYQ against MN at the molecular level. Methods: BZYQ components/targets were retrieved from TCMSP and UniProtKB, while MN-related targets were obtained from GeneCards and GEO. Core targets were identified via Protein-Protein Interaction (PPI) analysis and machine learning (ML). Immune cell infiltration was analyzed using CIBERSORT, and diagnostic values were evaluated via Receiver Operating Characteristic (ROC) curves. Molecular docking validated interactions between core targets and BZYQ's active ingredients, with efficacy and mechanisms further verified in a cationic bovine serum albumin-induced mouse MN model. Results: Screening identified *MYC* and *NFKBIA* as core targets, primarily enriched in B-cell receptor signaling. Immune infiltration analysis showed their correlation with follicular helper T cell abundance. ROC curves confirmed area under the curve > 0.7 for both targets. Molecular docking revealed strong binding (average energy: -7.13 kcal/mol) between targets and BZYQ components. In vivo, BZYQ significantly reduced 24-h urinary protein ($P < 0.001$), increased serum albumin ($P < 0.05$), decreased serum creatinine ($P < 0.05$), and alleviated renal pathology/immune complex deposition. Mechanistically, immunohistochemistry/Western blotting showed BZYQ downregulated MYC ($P < 0.05$) and upregulated IκBα ($P < 0.05$) versus the model group. Conclusion: BZYQ emerges as a promising therapeutic for MN. Elucidating its anti-MN mechanisms provides a theoretical basis for clinical translation.

Keywords: Bioinformatics analysis, immune cell infiltration, machine learning, animal experiments, membranous nephropathy, Buzhong Yiqi decoction

Introduction

Membranous nephropathy (MN) is one of the major causes of nephrotic syndrome in adults, with pathological features characterized by the deposition of immune complexes in the subepithelial space of the glomerular basement membrane (GBM), accompanied by diffuse thickening of the basement membrane [1]. These immune complexes are mainly composed of immunoglobulin G (IgG) and target antigens [2, 3]. Currently, in addition to basic treatments such as diuresis, antihypertensive therapy, lipid-lowering therapy, and anticoagulant therapy, the treatment of MN mainly relies on glucocorticoids combined with immunosuppressive agents and biologicals. However, long-term treatment with glucocorticoid hormones and immunosuppressants is often associated with varying degrees of side effects, as well as issues like poor patient compliance and heavy economic burden. Thus, there remains a press-

https://doi.org/10.62347/FFEN1563

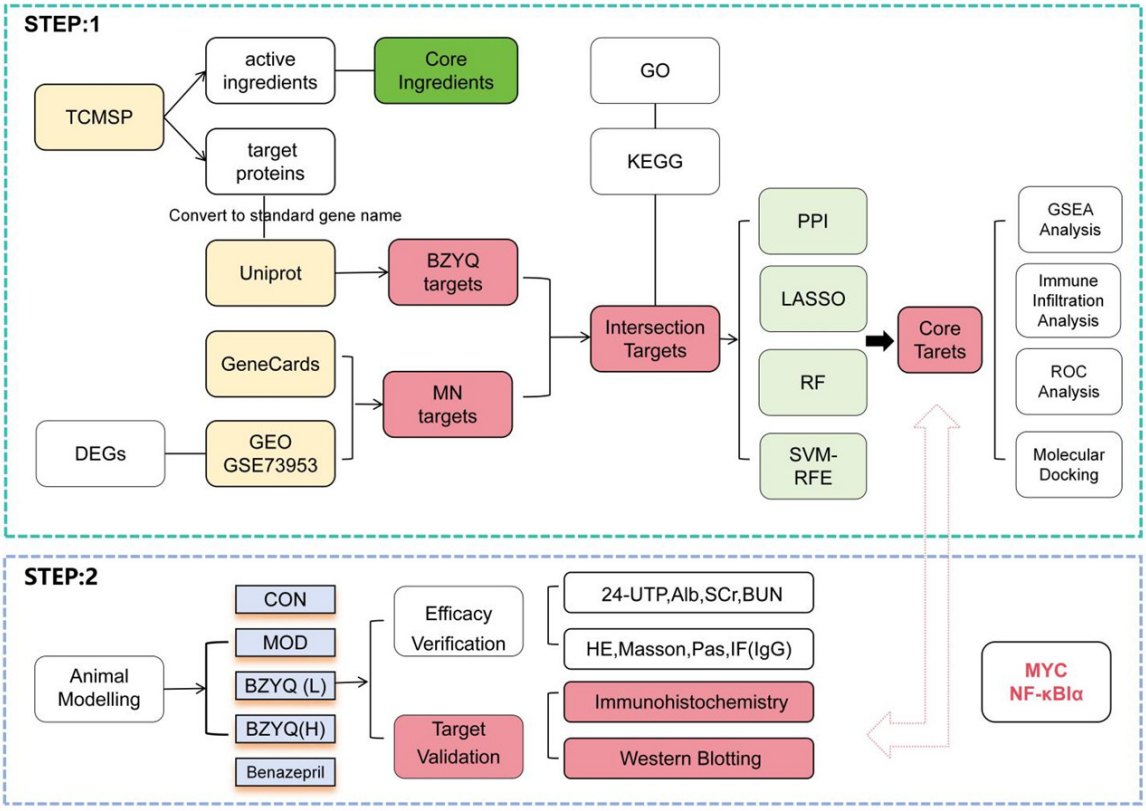

Figure 1. A flowchart summarizing the study design.

ing need to continuously explore novel therapeutic approaches.

Buzhong Yiqi Decoction (BZYQ) consists of eight Chinese herbs: Astragalus (Huangqi), Ginseng (Renshen), Atractylodes (Baizhu), Cimicifuga (Shengma), honey-fried Licorice (Zhigancao), Angelica sinensis (Danggui), Pericarpium Citri Reticulatae (Chenpi), and Bupleurum chinense (Chaihu). It is recognized for its efficacy in regulating spleen-stomach function [4], improving fatigue, enhancing immunity [5], and treating stress urinary incontinence [6]. Similarly, BZYQ has also demonstrated significant efficacy in the clinical management of MN [7], which provides a basis for BZYQ as a promising candidate drug for the treatment of MN. Nevertheless, the exact mechanism underlying the efficacy of BZYQ in MN has not been fully elucidated, warranting further analytical methods and multi-dimensional studies.

Network pharmacology constructs biological networks to integrate drug-target relationships and reveal multi-target mechanisms of action [8]. Machine Learning (ML) accurately identifies disease-related genes, signaling pathways, and functional proteins to facilitate new target discovery and drug efficacy prediction [9]. Molecular docking predicts molecular binding modes and affinities for drug discovery [10]. This study integrated the above methods and performed the following explorations (**Figure 1**).

(1) The active ingredients and corresponding targets of BZYQ were screened via the Traditional Chinese Medicine Systems Pharmacology Database and Analysis Platform (TCMSP) and Universal Protein Resource (UniProt), while the targets associated with MN were retrieved from the GeneCards and Gene Expression Omnibus (GEO).

(2) Protein-protein interaction (PPI) data among the targets were obtained from the Search Tool for the Retrieval of Interacting Genes (STRING) database, after which we constructed a PPI network to identify hub genes.

(3) Three algorithms of ML, namely Least Absolute Shrinkage and Selection Operator (LASSO), Random Forest (RF), and Support Vector Machine-Recursive Feature Elimination (SVM-RFE), were employed for further optimization to screen core genes.

(4) Gene Ontology (GO) and Kyoto Encyclopedia of Genes and Genomes (KEGG) enrichment analysis, immune infiltration analysis, and evaluation of diagnostic performance were performed on the core genes. Additionally, molecular docking was utilized to assess the binding affinity between core genes and active compounds, thereby validating their binding specificity.

(5) An animal model of MN was established to validate the therapeutic efficacy of BZYQ and the expression levels of core genes.

In summary, this study is designed to systematically explore and experimentally validate the therapeutic mechanism of BZYQ for treating MN, with the ultimate goal of providing novel therapeutic strategies and scientific theoretical support for clinical MN management.

Materials and methods

Screening for active ingredients and targets of BZYQ

The BZYQ active ingredients and their corresponding target proteins were obtained from the TCMSP (http://lsp.nwu.edu.cn/tcmsp.php). Considering that BZYQ tablets are administered orally, the screening criteria of Oral bioavailability (OB) ≥ 30% and drug-likeness (DL) ≥ 0.18 were adopted. The corresponding target proteins were subsequently mapped to their standard gene names through the UniProt (https://doi.org/10.1093/nar/gkaa1050).

Screening for MN target

MN-related targets were obtained from the GeneCards (http://www.genecas.org/) and the GEO (GSE73953) (http://www.ncbi.nlm.nih.gov/geo/). Differential analysis of the GSE73953 dataset was performed using the R package Limma, with adjusted *P*-values < 0.05 and |log2FC| > 0.58 set as screening criteria to identify upstream and downstream genes influencing MN progression.

Prediction of BZYQ targets for MN treatment

Based on the above information, drug-disease target intersections were plotted on the Venny 2.1 (http://bioinfogp.cnb.csic.es/tools/venny/), and component-target network diagrams were plotted using Cytoscape 3.7.1 software.

Construction of the PPI network

The intersection targets were imported into the STRING database (https://string-db.org/), and the filtering criteria of "Homo sapiens" species and "minimum interaction score" ≥0.9 were applied to remove isolated nodes. Subsequently, PPI data were exported in TSV format. The data were then imported into Cytoscape 3.7.1 software to generate a PPI network diagram, and the CytoHubba plugin was used to analyze the interactions among the targets to identify central targets (hubs).

GO and KEGG enrichment analysis

The intersection targets of BZYQ treatment for MN were imported into the Database for Annotation, Visualization and Integrated Discovery (DAVID, https://david.ncifcrf.gov/) for GO (biological process, BP; cellular component, CC; molecular function, MF) and KEGG enrichment analysis, and the results were visualized using Weishengxin online platform (http://www.bioinformatics.com.cn/).

Machine learning

To identify the core targets, we applied three algorithms - LASSO, RF, and SVM-RFE - to refine the key targets from the previously identified major drug-disease intersection targets. First, stringent 10-fold cross-validation was implemented using the glmnet package in R to enhance the model's robustness and reliability. Next, an RF classification model was built with the randomForest package, where key genes were prioritized according to the Gini index. Furthermore, the SVM-RFE algorithm was utilized via the e1071 and caret packages (with the "svmRadial" kernel) to further optimize feature selection, which effectively identified target genes with distinct expression profiles. Ultimately, by integrating the hub genes from PPI screening, we identified the potential core genes mediating the therapeutic effects of BZYQ in MN.

Gene set enrichment analysis (GSEA)

To assess the enrichment of core genes and identify their functional relevance, GSEA was conducted using the gseGO and gseKEGG functions from the clusterProfiler R package. This analysis evaluated the non-random enrichment of core genes within GO terms and KEGG pathways, ranking gene sets by their enrichment significance.

Immune-infiltration analysis

In this study, the GSE73953 dataset was analyzed using the CIBERSORT algorithm via its online platform to generate results. The relative proportions of 22 immune cell types in MN were then quantified using the Limma and dplyr packages. Subsequently, the ggpubr and ggExtra packages were employed to explore associations between the identified core targets and these immune-infiltrating cells, and the results were visualized to facilitate further analysis.

Receiver operating characteristic (ROC) curve

In this study, gene expression data from the GEO database GSE73953 were utilized to develop a training model. The model's performance was assessed using the pROC package in R, with ROC curves generated to visualize performance. The area under the curve (AUC) was calculated to measure the model's accuracy in differentiating MN patients from healthy controls.

Molecular docking

Molecular docking simulations were conducted to investigate the interactions between the active ingredients of BZYQ and core targets. It is worth noting that the presence of these compounds in the BZYQ formulation was experimentally validated via liquid chromatography-mass spectrometry (LC-MS) [11]. The 3D structures of target proteins were retrieved from the Protein Data Bank (PDB, https://www.wwpdb.org/) with a resolution threshold of ≤ 3.0 Å, with core active ingredients from the PubChem database (https://pubchem.ncbi.nlm.nih.gov/). These protein structures were preprocessed using PyMOL v3.0.4 to remove solvents and ligands, ensuring the proteins were in a suitable state for docking. Subsequently, molecular docking was performed using AutoDock 1.5.7 to simulate binding interactions, and the docking results were visualized using PyMOL3.0.

Animals

Thirty healthy female BALB/c mice (6-8 weeks old, 15-20 g) were obtained from Chengdu Pharmachem Biotechnology Co., Ltd. (Certificate of Conformity No. SCXK [Chuan] 2020-034). The animal experiment design and operating procedures of this study comply with the National Guidelines for the Care and Use of Laboratory Animals and have been approved by the Animal Ethics Committee of Southwest Medical University (Approval No.: 20221026-013). At the conclusion of animal experimentation, euthanasia was performed via intraperitoneal injection of a lethal dose of pentobarbital sodium (150 mg/kg) to ensure minimal suffering.

Modeling, grouping and drug administration

After one week of adaptive feeding, the mice were randomly divided into a normal group of 6 and a model group of 24. The administration method was as follows [12]: Pre-immunization for 2 weeks: 0.2 mg C-BSA (2 g/L) was fully emulsified with an equal volume of complete Freund's adjuvant (CFA) and the mixture was injected into mice in the model group via multipoint subcutaneous injection; mice in the normal group were given an equal amount of CFA. Formal immunization for 6 weeks: C-BSA (6.5 mg/kg) was administered to the model group mice via tail vein injection, and an equal amount of physiological saline was injected into the normal group. Two mice died during the modeling process. Subsequently, 24-hour urine protein (24-UP) levels of each mouse in the model group were measured, and all levels were greater than 60 μg/day, indicating abnormal proteinuria [13]. Two mice were randomly selected for renal tissue immunofluorescence assay, and both exhibited IgG immune complex deposition, confirming the validity of the model. The remaining 20 model mice were randomly divided into four groups: a model group, a BZYQ high-dose group (7.42 g/kg), a BZYQ low-dose group (3.71 g/kg), and a Captopril group (1.3 mg/kg), with 5 mice in each group. The corresponding dose of the drug was administered orally once daily for 1 month.

Determination of biochemical indexes in mice

Prior to sampling, each mouse was individually placed in a metabolic cage for 24-hour urine collection, with group information recorded accordingly. Mouse urine samples were centrifuged at 4,000 rpm for 10 minutes (centrifuge radius: 10 cm), and 24-UP was measured following the instructions provided with the urine protein assay kit. After sampling, serum was collected from each group of mice, allowed to stand overnight, and centrifuged at 4,000 rpm for 10 minutes (centrifuge radius: 10 cm). We took the supernatant and measured the levels of albumin (Alb), serum creatinine (SCr), and blood urea nitrogen (BUN) according to the instructions of the corresponding reagent kit.

Histopathological analysis of the kidney

The tissues were fixed in 4% paraformaldehyde, then dehydrated, embedded in paraffin, sectioned, and stained with HE, Masson, and PAS stains, and the morphological changes of renal tissues were observed under a light microscope.

Detection of IgG deposition in the mouse kidney

Fresh kidney tissues were embedded in OCT embedding medium and immediately placed into a -20°C cryostat for sectioning. Sections were cut to a thickness of 4 μm, fixed in acetone for 5 minutes, and then washed three times with phosphate-buffered saline (PBS). The sections were soaked in 5% bovine serum albumin (BSA) blocking buffer before incubation with FITC-labeled mouse IgG antibody in the dark overnight. On the following day, the sections were brought to room temperature, washed again with PBS, mounted with glycerol, and air-dried. The sections were then examined under a fluorescence microscope and imaged.

Immunohistochemistry

Following deparaffinization, hydration, and antigen retrieval, kidney sections were blocked with 5% BSA and subsequently incubated overnight with primary antibodies against MYC and IκBα. The following day, the sections were washed with PBS, incubated with horseradish peroxidase (HRP)-conjugated corresponding secondary antibodies at room temperature for 1 h, stained with 3,3'-diaminobenzidine (DAB) and counterstained with hematoxylin.

Western blotting

Kidney tissues were homogenized in 400 μL of RIPA lysis buffer supplemented with 100 mmol/L PMSF. The protein concentration was determined and adjusted to 10 μg/μL using a microplate reader. Subsequently, protein samples were denatured in SDS loading buffer at 100°C for 10 min. 10 μL of each protein sample was subjected to SDS-PAGE on a 10% polyacrylamide gel and then electrotransferred onto a PVDF membrane. The membrane was blocked with 5% BSA in TBST at room temperature for 1 h, followed by incubation with primary antibodies (GAPDH 1:10,000, MYC 1:1,000, IκBα 1:1,000) at 4°C overnight. After washing with TBST, the membrane was incubated with corresponding horseradish peroxidase-conjugated IgG secondary antibody at room temperature for 1 h and washed again with TBST. Chemiluminescence was detected using ECL chemiluminescence substrate, and the membrane was imaged using the Qinxiang imaging system. The relative gray value ratio of the target protein to the internal control was quantified using ImageJ software.

Statistical analysis

Statistical data analysis was performed using GraphPad Prism 9.0 statistical software. Quantitative data were described, and intergroup comparisons were performed using one-way ANOVA. Unless otherwise specified, the significance level α was set at 0.05.

Results

Main target screening and component-target network diagram establishment

A total of 131 active ingredients of BZYQ were screened by TCMSP, and 232 active targets were obtained by querying the action targets of the above active ingredients and removing the duplicates; 1,840 MN-related target genes were screened by GEO-DEGs, of which 1,174 were up-regulated and 666 were down-regulated (**Figure 2A**); 4,478 MN targets were screened by GeneCards; 16 major targets of BZYQ for MN treatment were identified by taking the intersection of the three sets of data (**Figure**

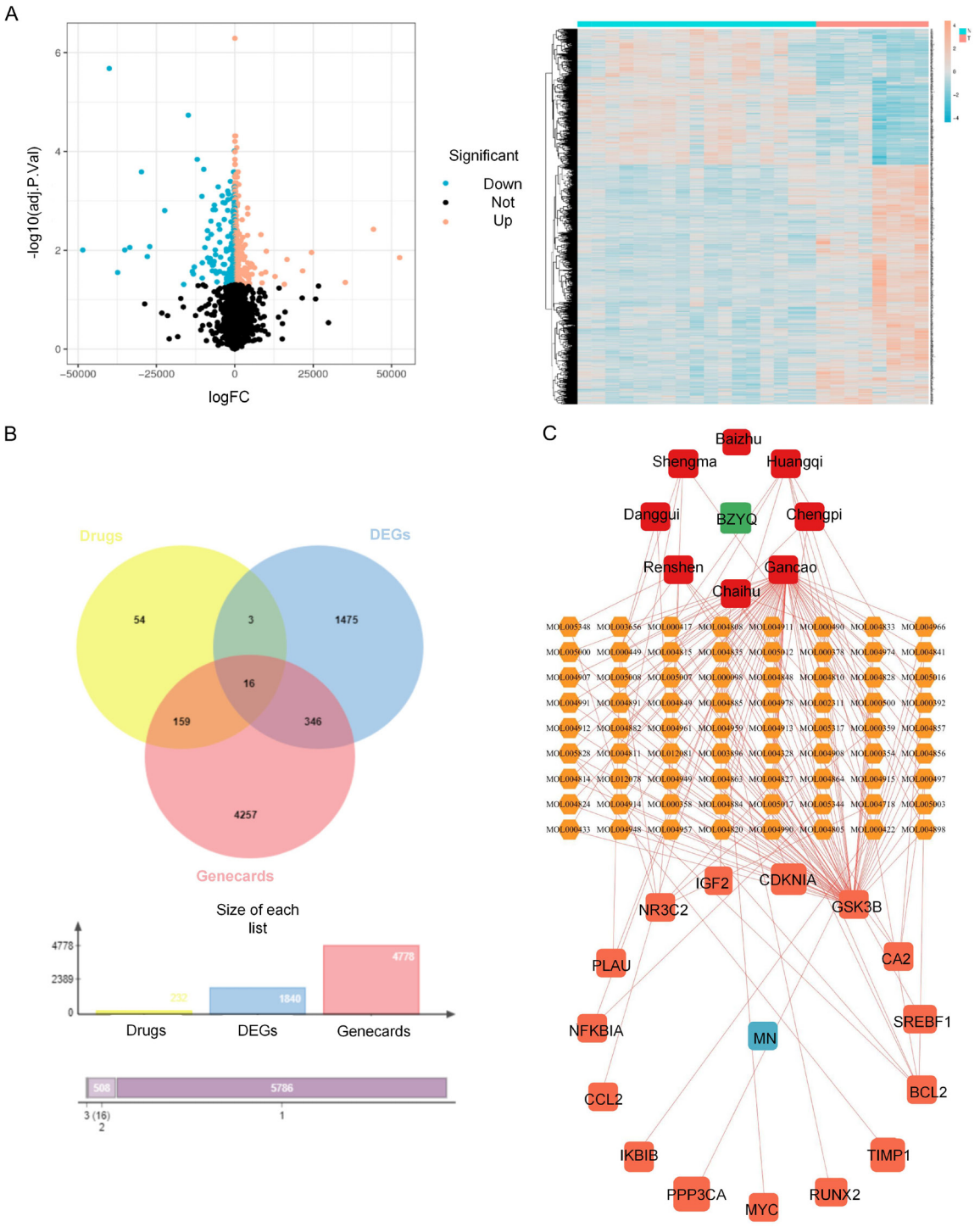

Figure 2. Expression profile of the GSE73953 dataset. A. Volcano map of detected genes. Each dot represents a gene. Blue dots represent downregulated genes, and pink dots represent upregulated genes. The screening criteria for significant genes were |log2FC| > 1 and P < 0.05. B. Heatmap display of the clustering of the differentially expressed genes (DEGs). Blue represents low expression, pink represents high expression. C. BZYQ-component-target network. The Chinese medicines are depicted as red rectangle nodes, their compounds as yellow ellipse nodes, and the disease genes as orange polygon nodes.

2B). Finally, a total of 68 components corresponding to 16 major targets were found among the 131 active ingredients of BZYQ; a component-target gene network diagram (**Figure 2C**)

Table 1. Information on the core components of BZYQ

Mol ID	Molecule name	OB%	DL	Drug
MOL000422	kaempferol	41.88	0.24	HQ TSZ YMC
MOL000098	quercetin	46.43	0.28	HQ TSZ GQZ HL
MOL000449	Stigmasterol	48.03	0.76	SD GQZ
MOL000497	licochalcone a	40.79	0.29	GC JXT
MOL004328	naringenin	59.29	0.21	BH CP GC

was constructed, and the core components of BZYQ were identified based on the number of interactions: quercetin, kaempferol, stigmasterol, and licochalcone a (**Table 1**).

PPI network analysis

The 16 targets common to diseases and drugs were entered into the STRING database to obtain a preliminary PPI network (**Figure 3A**). This work was then imported into Cytoscape 3.7.1 software, and the topological attributes of the PPI network were analyzed using the "NetworkAnalyzer" module. The color shades of the nodes were positively correlated with the size of the degree value (**Figure 3B**). The color depth of nodes was positively correlated with the degree value, the larger the degree value, the darker the color. As a result, the core targets in the network were identified as *BCL2, MYC, NFKBIA* (The *NFKBIA* gene encodes IκBα, an inhibitor of nuclear factor kappa B alpha)*, CCL2, and GSK3β* (**Table 2**).

Enrichment analysis

GO and KEGG analysis was performed on 16 targets using the DAVID platform, and the results with the lowest *P*-values (i.e., the most significant results) were selected for visualization. The results showed that the highly relevant signaling pathways include: Lipid and atherosclerosis pathway, B-cell receptor signaling pathway, IL-17 signaling pathway, PI3K-Akt signaling pathway, and MAPK signaling pathway (**Figure 3C**). Additionally, the results showed that BPs were mainly involved in cellular responses to peptides, responses to peptide hormone, positive regulation of cellular activation and responses to exogenous stimuli; CCs were mainly involved in macromolecular complexes such as Bcl-2 family protein complex, CD40 receptor complex, peptidase inhibitor complex, RNA polymerase II transcriptional repressor complex and macromolecular complexes; MFs were mainly involved in DNA-binding transcription factor binding, NF-κB binding and binding to various enzyme (**Figure 3D** and **3E**).

Machine learning

The LASSO algorithm narrowed down the initial 16 genes to 8 key genes (**Figure 4A**). Meanwhile, the RF algorithm assigned an importance score to each gene; and a threshold of 0.1 was set, resulting in the identification of 12 key genes (**Figure 4B**). In addition, the SVM-RFE algorithm identified 9 genes, achieving a peak classification accuracy of 1 and a minimum RMSE of 0 (**Figure 4C**). By taking the intersection of the above three gene sets with the five core targets screened from PPI, two key genes were obtained: *NFKBIA* and *MYC* (**Figure 4D**).

GSEA

Through individual GSEA analysis performed on the two core targets, their corresponding functional attributes and associated pathways were obtained (**Figure 5A** and **5B**). It was found that both targets were enriched in the B-cell receptor (BCR) signaling pathway, and the mechanism of the B-cell receptor pathway is illustrated in **Figure 5C**.

Analysis of immune infiltration

The level of each immune cell infiltration in MN was assessed. It was found that naive B cells and M2 macrophages had higher proportions in MN compared with those in the control group, and their activations might be involved in the pathogenesis of MN (**Figure 6A**). Meanwhile, all of these immune cells were correlated with core targets to varying degrees, as presented in the corresponding heatmap (**Figure 6B** and **6C**). *MYC* is strongly associated with naive B cells and mast cell activation, whereas *NFKBIA* exhibits a strong association with neutrophils and regulatory T cells. Additionally, both MYC and *NFKBIA* are strongly associated with follicular helper T cells (Tfhs).

ROC curve analysis

The ROC curve was plotted to demonstrate the diagnostic performance of the same model under different conditions and the diagnostic

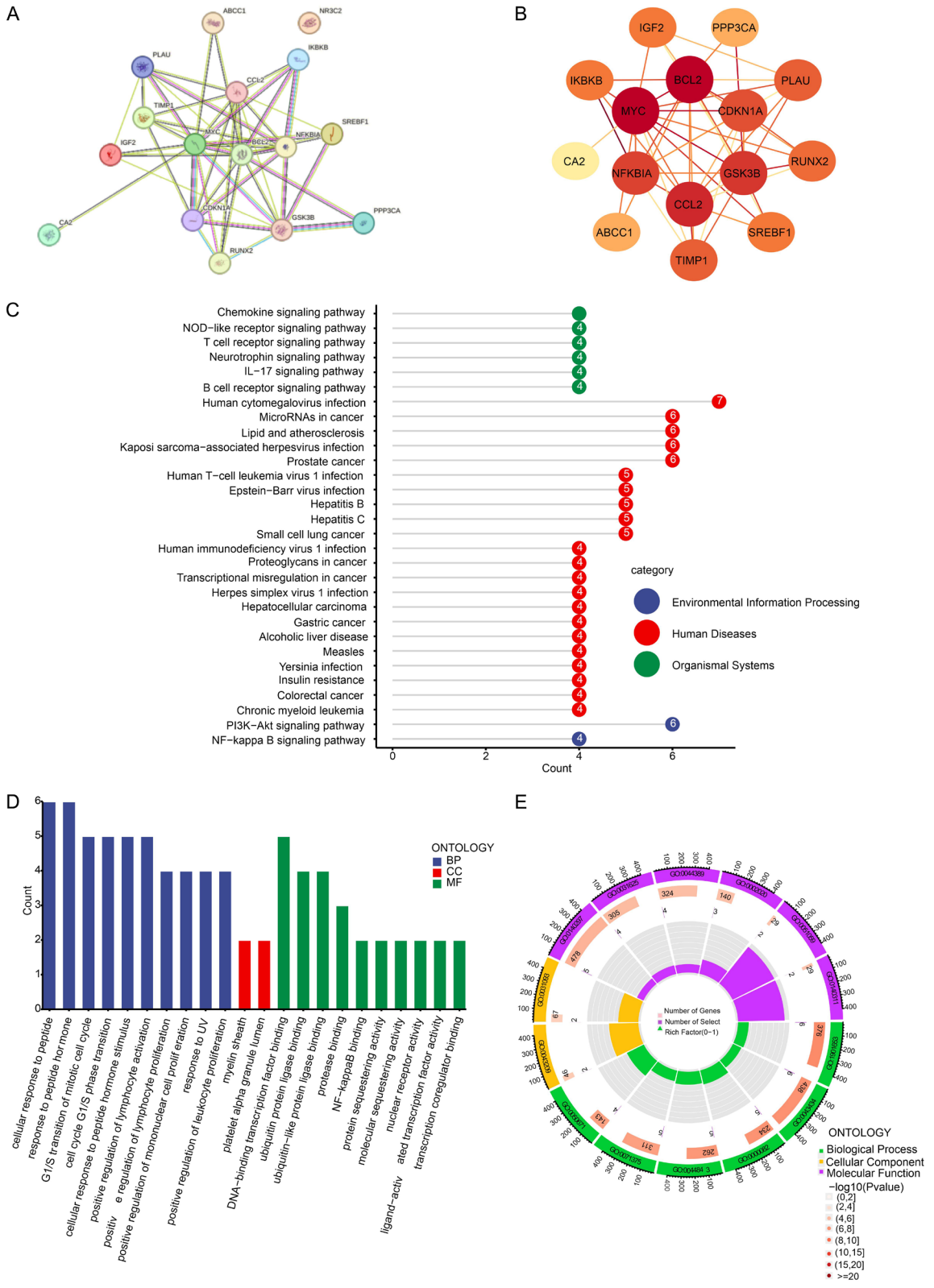

Figure 3. A. Protein-Protein Interaction (PPI) of BZYQ targets for treating MN from STRING. B. PPI network processed using Cytoscape. C. Signaling pathways identified from Kyotoencyclopedia of genes and genomes (KEGG) analysis. D, E. Results of Gene Ontology (GO) Enrichment Analysis.

Table 2. Core targets information

Number	Rank	Gene name	Protein name	Degree
1	1	BCL2	B-cell lymphoma 2 protein	13
2	1	MYC	Myc proto-oncogene protein	13
3	3	CCL2	Chemokine (C-C motif) ligand 2	10
4	4	GSK3β	Glycogen Synthase Kinase 3 Beta	9
5	5	NFKBIA	NF-kappa-B inhibitor alpha	8

performance of the two core genes. Analysis revealed that the AUC values of the model under non-interference and interference conditions were 0.758 and 0.641, respectively (**Figure 6C** and **6D**), indicating that the data as a whole had good diagnostic capability. The AUC values of *MYC* and *NFKBIA* were greater than 0.7 (**Figure 6E** and **6F**), indicating that the two genes exhibit good sensitivity and specificity.

Molecular docking

The core components of BZYQ were molecularly docked with MYC and IκBα (encoded by NFKBIA), and it was found that each component had a good binding affinity with these proteins, with an average binding energy of -7.13 kcal/mol. The results were visualized (**Figure 7A-F**), and the heatmap is presented in **Figure 7G**.

Protective effect of BZYQ on MN in mice

Compared with the normal group, mice in the model group exhibited significantly increased 24h-UP ($P < 0.001$) and SCr ($P < 0.01$) levels, along with significantly decreased Alb ($P < 0.001$) levels, all with statistically significant differences. Although BUN levels were increased, the difference was not statistically significant ($P > 0.05$). In contrast, compared with the model group, mice treated with BZYQ or captopril showed significantly decreased 24h-UP ($P < 0.001$) and SCr ($P < 0.05$) levels, as well as significantly increased, Alb levels ($P < 0.05$), with all these changes reaching statistical significance. BUN levels were decreased, but the difference was not statistically significant ($P > 0.05$) (**Figure 8A-D**).

BZYQ attenuates kidney injury in mice

In addition, the effect of BZYQ on renal histopathology in MN mice was assessed by HE staining, Masson staining, and PAS staining. It was found that the normal group of mice had an intact structure and a normal size of the tubular lumen, while the model group showed increased glomerular volume, mesangial cell proliferation, and basement membrane thickening. The degree of pathological damage was significantly reduced in the BZYQ-treated groups (**Figure 8E**).

IgG deposition in mouse kidney tissue

Under identical imaging conditions, no immune complex deposition was observed in the normal group. In contrast, the model group exhibited a substantial amount of IgG deposited diffusely along the capillary loops, which displayed intense fluorescence. In the BZYQ-treated groups, the IgG deposition was diminished, and the fluorescence intensity was attenuated (**Figure 9A**).

Effect of BZYQ on MYC and IκBα protein expression

A significant difference was observed in the expression of core proteins MYC and IκBα in normal and model tissues by immunohistochemistry. Compared with the normal group, the MYC level was increased and the IκBα level was decreased in the model group; BZYQ and Benazepril HCl significantly decreased MYC ex pression and increased IκBα expression compared with the model group (**Figure 9B**).

Western blot further validated that MYC expression levels were significantly increased ($P < 0.05$) in the model group compared with the control group while that of IκBα was significantly decreased ($P < 0.05$). However, BZYQ reversed these abnormal changes (**Figure 9C**).

Discussion

Currently, the clinical management of MN primarily relies on immunosuppressive therapies, including cyclophosphamide combined with corticosteroids, calcineurin inhibitors, and CD20-targeted B-cell depletion strategies. However, these interventions are frequently constrained by adverse reactions and high recurrence rates [14, 15]. Notably, patients refrac-

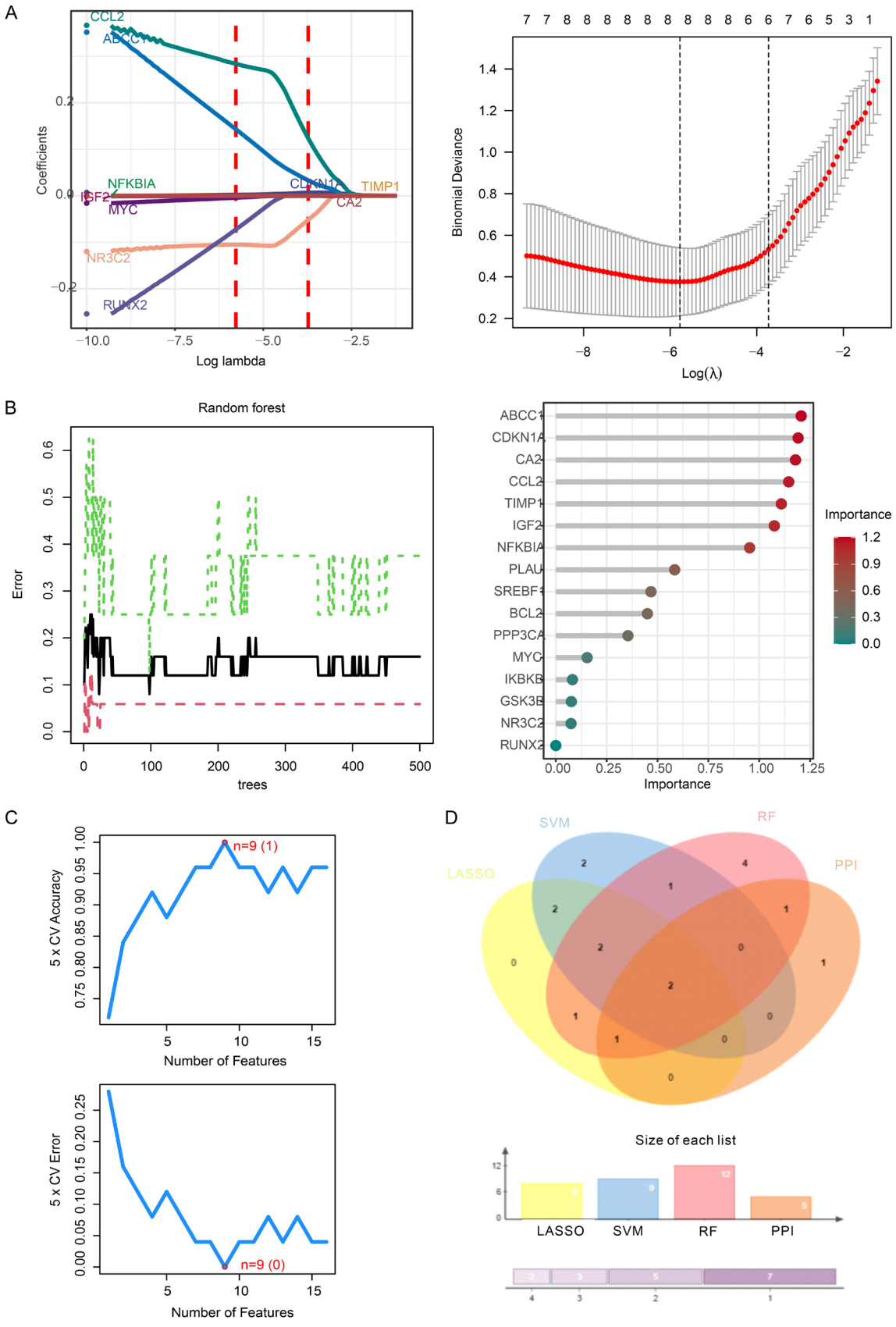
A
CCL2
ABCC1
NFKBIA
IGF2
MYC
CDKN1A
TIMP1
CA2
NR3C2
RUNX2
Coefficients
Log lambda
Binomial Deviance
Log(λ)
B
Random forest
Error
trees
ABCC1
CDKN1A
CA2
CCL2
TIMP1
IGF2
NFKBIA
PLAU
SREBF1
BCL2
PPP3CA
MYC
IKBKB
GSK3B
NR3C2
RUNX2
Importance
C
5 x CV Accuracy
n=9 (1)
Number of Features
5 x CV Error
n=9 (0)
D
SVM
RF
LASSO
PPI
Size of each list

Figure 4. A. Screening for core genes using the Least absolute shrinkage and selection operator (LASSO). B. Screening for core genes using the random forest algorithm (RF). C. Screening for core genes using the Support Vector Machine-Recursive Feature Elimination (SVM-RFE). D. Core target genes identified via integration of three machine learning (ML) methods and PPI network analysis.

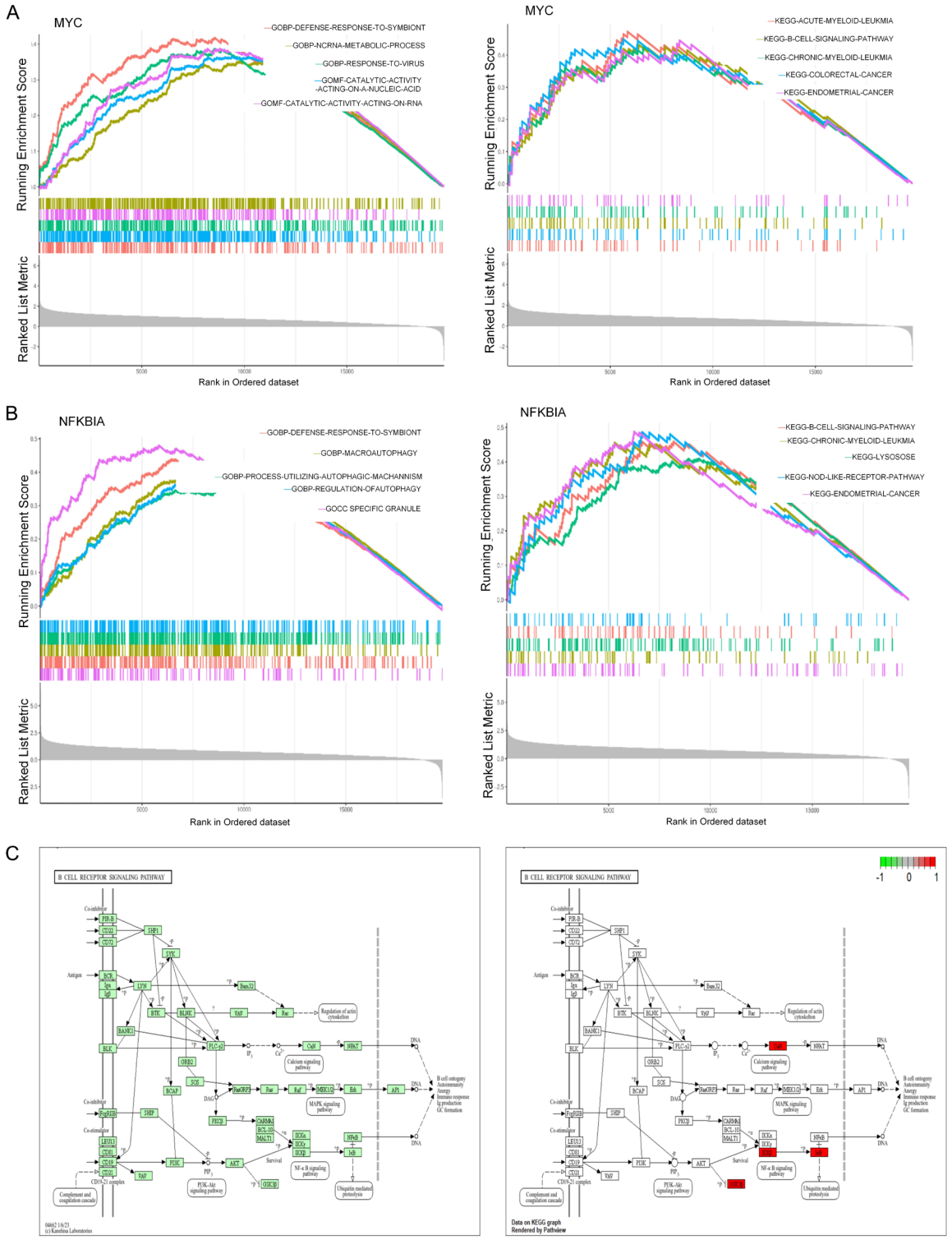

Figure 5. A. GSEA-GO/KEGG of MYC. B. GSEA-GO/KEGG of NFKBIA. C. B-cell receptor pathway mechanisms.

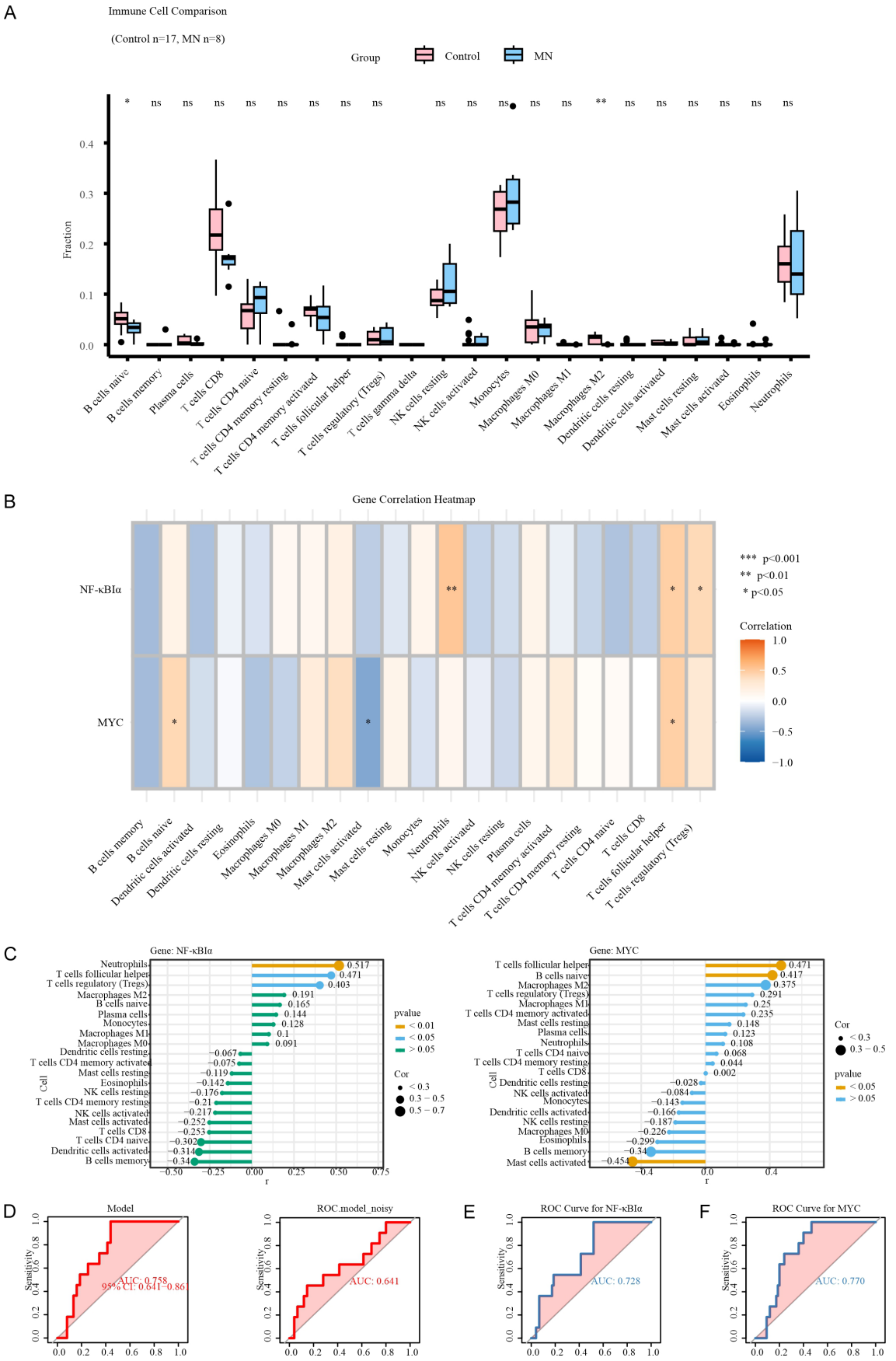
A
Immune Cell Comparison
(Control n=17, MN n=8)
Group
Control
MN
Fraction
B cells naive
B cells memory
Plasma cells
T cells CD8
T cells CD4 naive
T cells CD4 memory resting
T cells CD4 memory activated
T cells follicular helper
T cells regulatory (Tregs)
T cells gamma delta
NK cells resting
NK cells activated
Monocytes
Macrophages M0
Macrophages M1
Macrophages M2
Dendritic cells resting
Dendritic cells activated
Mast cells resting
Mast cells activated
Eosinophils
Neutrophils
B
Gene Correlation Heatmap
NF-κBIα
MYC
*** p<0.001
** p<0.01
* p<0.05
Correlation
C
Gene: NF-κBIα
Gene: MYC
Cell
r
pvalue
Cor
D
Model
ROC.model_noisy
Sensitivity
AUC: 0.758
95% CI: 0.641−0.861
AUC: 0.641
E
ROC Curve for NF-κBIα
AUC: 0.728
F
ROC Curve for MYC
AUC: 0.770

Figure 6. A. Immune cell infiltration analysis evaluated the abundance of 22 immune cells in control and MN groups using ssGESA in the GSE73953 dataset. B, C. Relevance of immune cells to MYC and NFKBIA. D. The performance of the MN diagnostic model. E, F. ROC analysis of MYC and NFKBIA.

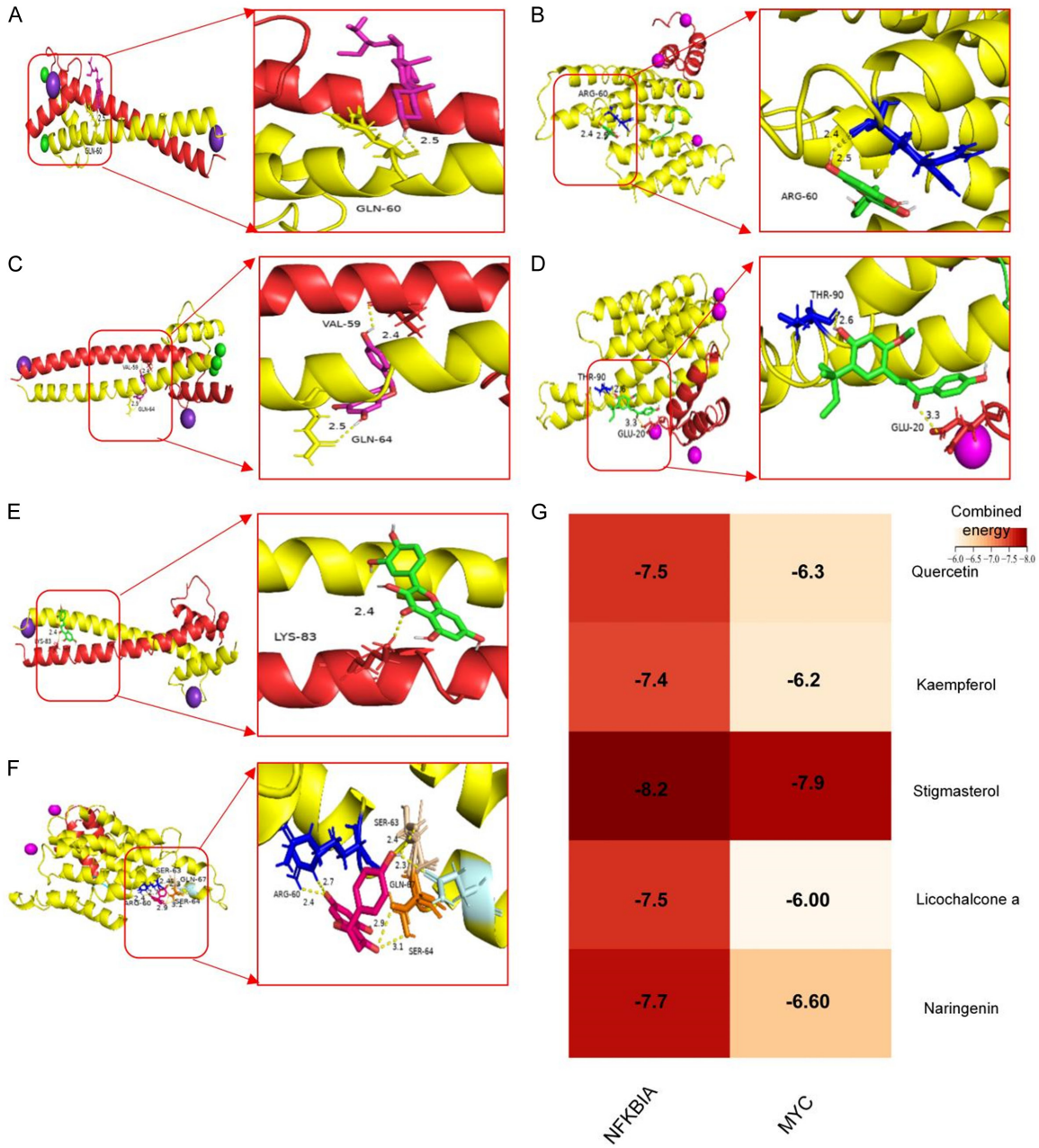

Figure 7. Visualization of molecular docking between core targets and components. A. MYC and Stigmasterol. B. IκBα and Kaempferol. C. MYC and Naringenin. D. IκBα and Licochalcone a. E. MYC and Quercetin. F. IκBα and Naringenin. G. Docking thermal diagram of the main components of BZYQ with MYC and IκBα.

tory to immunosuppressive agents may experience accelerated progression to end-stage renal disease (ESRD) [16]. In recent years, the efficacy of traditional Chinese medicine in improving renal function and treating MN has gained increasing recognition [17, 18]. Against this backdrop, the present study aims to integrate bioinformatics, network pharmacology, and ML approaches to investigate the potential therapeutic mechanisms of the classic tradi-

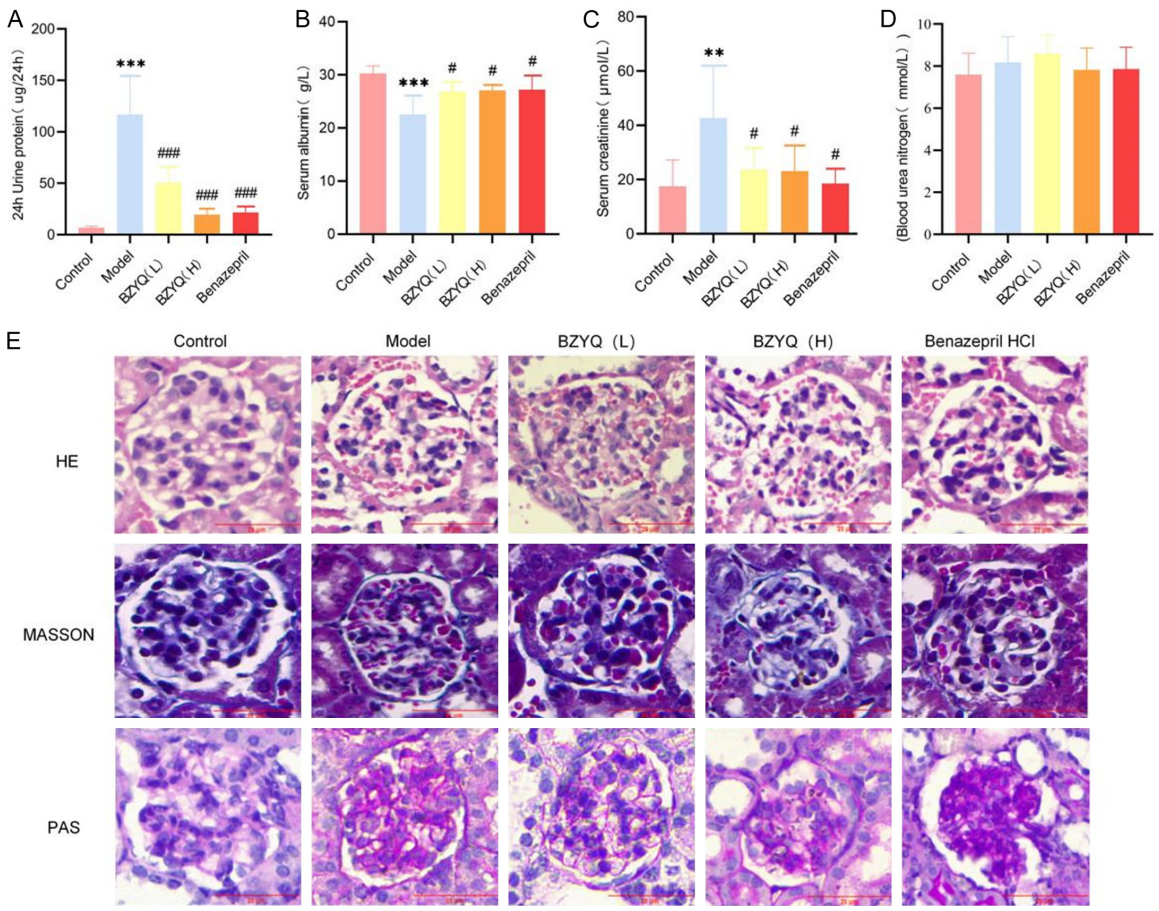

Figure 8. Changes in biochemical indicators and pathological alterations in mice of each group. A. The 24-hour urine protein quantification (24-UP). B. Serum albumin (Alb). C. Creatinine (Scr). D. Blood Urea Nitrogen (BUN). ***P < 0.001, **P < 0.01 compared to the Control; #P < 0.05, ###P < 0.001 compared to the Model. E. HE, Masson, Pas staining results of mouse kidney tissue (original magnification ×400).

tional formula BZYQ, thereby providing additional options for clinical practice.

The core components of BZYQ identified in our study include kaempferol, quercetin, stigmasterol, Licochalcone A, and naringin, among others. Experimental evidence has demonstrated that these components not only exert inhibitory effects on inflammatory responses [19-22] but also possess significant anti-fibrotic activity in various disease settings [23-25]. Such properties underscore their potential therapeutic significance in chronic kidney disease, prompting the hypothesis that these components may play a pivotal role in the therapeutic effects of BZYQ against MN.

Ultimately, *MYC* and *NFKBIA* were identified as the core targets of BZYQ in the treatment of MN. As a key nuclear transcription factor, MYC has been demonstrated to regulate the expression of numerous human genes and is extensively involved in various physiological processes, including cell growth, differentiation, and apoptosis [26]. Research has indicated that MYC overexpression significantly mediates inflammatory responses in glomerular endothelial cells in both diabetic nephropathy patients and rat models [27]. The NF-κB pathway is widely implicated in immune and inflammatory responses, and it can mediate renal inflammation in various cell types [28]. As the core negative regulator in the NF-κB signaling pathway, IκBα is capable of binding to NF-κB in the resting state and preventing its translocation to the nucleus - thereby inhibiting the transcriptional activity of NF-κB [29] and playing a key role in alleviating renal inflammation [30]. The close relationship between core targets and inflammation regulation coincides with the pathogen-

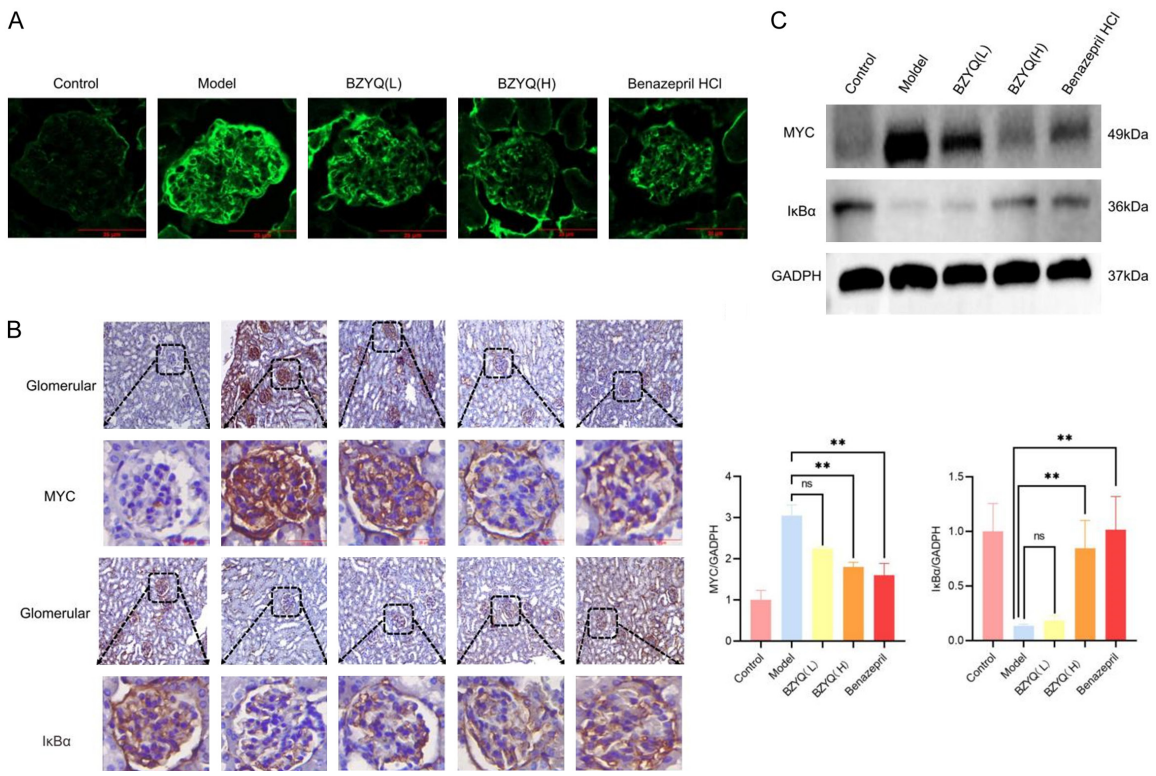

Figure 9. A. IgG deposition in mouse kidney tissue (original magnification ×400). B. Immunohistochemistry staining of MYC and IκBα (original magnification ×400). C. Protein expression levels of MYC and IκBα in kidney tissue were determined using Western blotting. Relative quantitative analysis of MYC and IκBα expression.

esis of MN [31, 32]. In addition, activation of podocyte autophagy has been shown to mitigate podocyte injury and exert renal protective effects [33]. Prior studies have clarified that MYC expression regulates autophagy [34]. Moreover, MYC is highly expressed in multiple kidney diseases, and targeted reduction of MYC can exert dual effects of anti-inflammation and autophagy promotion [26, 35, 36]. These findings further underscore its potential as a key therapeutic target for MN.

Next, we performed single-cell enrichment analysis on two core targets, which revealed that these targets are closely associated with the BCR signaling pathway. Abnormal BCR signaling or elevated BAFF levels are known to induce B cell activation and differentiation into plasma cells, leading to the secretion of large amounts of autoantibodies and thereby promoting the progression of MN [37]. Notably, MYC expression is often accompanied by the activation of BCR signaling pathway-related proteins, including CD79α, Btk, Plcγ2, and Erk1/2 [38]. Based on these findings, we hypothesize that MYC may promote B cell survival and proliferation by enhancing the activity of the BCR signaling pathway, thereby participating in the pathogenesis of MN. Subsequent immune infiltration analysis revealed a significant association between the two core targets and Tfhs. Tfhs is involved in immune dysfunction in MN, and its subpopulation imbalance induces B cell differentiation and plays a key role in the pathological process of MN [39, 40]. Additionally, ROC curve analysis demonstrated that *MYC* and *NFKBIA* exhibit favorable diagnostic performance, while molecular docking results indicated that MYC and IκBα form favorable binding interactions with the key active components of BZYQ. All these results suggest that these two core targets are promising candidates for further investigation.

Based on the above screening results, we selected female mice, which are more likely to produce typical pathological changes and clinical manifestations, to establish a model of MN [41]. Through biochemical and histopathological analysis, we found that compared with the

control group, BZYQ administration significantly reduced the 24-hour urine protein level and increased the serum albumin level in mice, alleviated pathological damage, and reduced the expression of IgG, the main immune deposit antibody in MN [42]. Additionally, both IHC and WB analyses showed significant differences in the expression of two core proteins, MYC and IκBα, between the control and model groups, with positive changes observed after BZYQ administration. This suggests that BZYQ may target MYC and IκBα in the treatment of MN.

A key advantage of this study is the integration of traditional network pharmacology with ML. By analyzing data via algorithms, this integration partially addresses the limitations encountered in identifying new drug targets in network pharmacology due to technical and knowledge limitations, as well as poor-quality databases [43]. Additionally, various bioinformatics methods were employed to further validate the associations between core genes, drugs, and diseases. A limitation of this study is that the protein expression of core genes was only validated via in vivo experiments. Future research should further optimize in vitro experiments and pathway mechanism validation.

Conclusion

In summary, BZYQ exerts therapeutic effects on renal injury in MN by modulating the expression of MYC and IκBα. These findings offer valuable insights into the clinical application of BZYQ. Future studies should focus on validating these findings through experimental modeling. Additionally, an in-depth investigation of its long-term effects and potential interactions with other therapeutic agents will provide a crucial foundation for a comprehensive assessment of its clinical application potential.

Acknowledgements

We would like to express our sincere gratitude to the Centre for Research on the Integration of Chinese and Western Medicine at the Traditional Chinese Medicine Hospital Affiliated to Southwest Medical University, the Animal Experimentation Centre of Southwest Medical University, and the Traditional Chinese Medicine Pharmacy at the Traditional Chinese Medicine Hospital Affiliated to Southwest Medical University for their invaluable and strong support throughout this research. This work was supported by the Sichuan Science and Technology Program (2025ZNSFSC0617).

Disclosure of conflict of interest

None.

Abbreviations

BZYQ, Buzhong Yiqi decoction; MN, membranous nephropathy; GEO, Gene Expression Omnibus; DEG, Differential expression gene; OB, Oral bioavailability; DL, drug-likeness; PPI, Protein-Protein Interaction; GO, Gene ontology; KEGG, Kyotoencyclopedia of genes and genomes; GSEA, Gene set enrichment analysis; ML, Machine learning; LASSO, Least absolute shrinkage and selection operator; RF, Random forest; SVM-RFE, Support Vector Machine-Recursive Feature Elimination; ROC, Receiver operating characteristic curve; AUC, Area under curve; Tfhs, follicular helper T cells.

Address correspondence to: Dr. Junming Fan, Department of Nephrology, The First Affiliated Hospital of Chengdu Medical College, Chengdu 610500, Sichuan, China. Tel: +86-18980601061; E-mail: junmingfan@163.com; Dr. Li Wang, Research Center of Integrated Traditional Chinese and Western Medicine, The Affiliated Traditional Chinese Medicine Hospital of Southwest Medical University, Luzhou 646000, Sichuan, China. Tel: +86-15182510560; E-mail: wangli111@swmu.edu.cn

References

[1] Ronco P, Beck L, Debiec H, Fervenza FC, Hou FF, Jha V, Sethi S, Tong A, Vivarelli M and Wetzels J. Membranous nephropathy. Nat Rev Dis Primers 2021; 7: 69.

[2] Sethi S and Fervenza FC. Membranous nephropathy-diagnosis and identification of target antigens. Nephrol Dial Transplant 2024; 39: 600-606.

[3] Sethi S. New 'Antigens' in membranous nephropathy. J Am Soc Nephrol 2021; 32: 268-278.

[4] Hu Q, Chen XP, Tang ZJ, Zhu XY and Liu C. Therapeutic effects of Buzhong Yiqi decoction in patients with spleen and stomach qi deficiency after routine surgery and chemotherapy for colorectal cancer. World J Gastrointest Surg 2024; 16: 2183-2193.

[5] Hu J, Li X, Fang Y and Peng J. Efficacy and safety of Buzhong Yiqi Decoction in improving cancer-related fatigue and immunity of cervical

carcinoma patients: a protocol of randomized controlled trial. Medicine (Baltimore) 2021; 100: e27938.
[6] Wang Y, Chen Y, Ma X, Guan J, Gao Y, Hong X, Fu P and Zhou F. Apo E protein and related markers show the prognosis of stress urinary incontinence rats treated with modified Buzhong Yiqi Decoction. Int J Biol Macromol 2024; 280: 135996.
[7] Gao YW, Wang XH, Yang HJ, Hu XH, Cui HR, Xu BZ, Li DL and Wang T. Clinical observation on modified Buzhong Yiqi Decoction combined with Guizhi Decoction in the treatment of idiopathic membranous nephropathy. Chinese Journal of Integrated Traditional and Western Nephrology 2020; 21: 343-345.
[8] Tie D, He M, Li W and Xiang Z. Advances in the application of network analysis methods in traditional Chinese medicine research. Phytomedicine 2025; 136: 156256.
[9] Vadapalli S, Abdelhalim H, Zeeshan S and Ahmed Z. Artificial intelligence and machine learning approaches using gene expression and variant data for personalized medicine. Brief Bioinform 2022; 23: bbac191.
[10] Paggi JM, Pandit A and Dror RO. The art and science of molecular docking. Annu Rev Biochem 2024; 93: 389-410.
[11] Li RS, Liu W, Pan Z, Zhang YJ, Zhang JJ, Zhang LZ and Yuan WA. Identification of chemical components in Buzhong Yiqi Decoction and their distribution characteristics in mice by UHPLC-Q-Exactive Orbitrap HRMS. Chinese Traditional and Herbal Drugs 2025; 56: 3041-3057.
[12] Wu CC, Chen JS, Chen SJ, Lin SH, Chen A, Chang LC, Sytwu HK and Lin YF. Kinetics of adaptive immunity to cationic bovine serum albumin-induced membranous nephropathy. Kidney Int 2007; 72: 831-40.
[13] Song XW, Quan ZL, Zang HL and Guo CK. MicroRNA-19b-3p targets the JAK2-STAT1 signaling pathway to regulate the Th17/Treg immune balance in a mouse model of membranous nephropathy. J Clin Neurol 2025; 25: 327-336.
[14] Ronco P, Beck L, Debiec H, Fervenza FC, Hou FF, Jha V, Sethi S, Tong A, Vivarelli M and Wetzels J. Membranous nephropathy. Nat Rev Dis Primers 2021; 7: 69.
[15] Buse M, Dounousi E, Kramann R, Floege J and Stamellou E. Newer B-cell and plasma-cell targeted treatments for rituximab-resistant patients with membranous nephropathy. Clin Kidney J 2025; 18: sfaf088.
[16] Shiiki H, Saito T, Nishitani Y, Mitarai T, Yorioka N, Yoshimura A, Yokoyama H, Nishi S, Tomino Y, Kurokawa K and Sakai H; Research Group on Progressive Renal Diseases in Japan. Prognosis and risk factors for idiopathic membranous nephropathy with nephrotic syndrome in Japan. Kidney Int 2004; 65: 1400-7.
[17] Zhu H, Xiao Y and Ji Y. Efficacy and safety of Chinese herbal medicines combined with biomedicine in the treatment of idiopathic membranous nephropathy: a systematic review and network meta-analysis. Front Pharmacol 2024; 15: 1391675.
[18] Lang R, Wang X, Liang Y, Yan L, Shi B and Yu R. Research progress in the treatment of idiopathic membranous nephropathy using traditional Chinese medicine. J Transl Int Med 2020; 8: 3-8.
[19] Wang Z, Sun W, Sun X, Wang Y and Zhou M. Kaempferol ameliorates cisplatin induced nephrotoxicity by modulating oxidative stress, inflammation and apoptosis via ERK and NF-κB pathways. AMB Express 2020; 10: 58.
[20] la Torre Fabiola VD, Ralf K, Gabriel B, Victor Ermilo AA, Martha MG, Mirbella CF and Rocio BA. Anti-inflammatory and immunomodulatory effects of Critonia aromatisans leaves: down-regulation of pro-inflammatory cytokines. J Ethnopharmacol 2016; 190: 174-82.
[21] Lv H, Yang H, Wang Z, Feng H, Deng X, Cheng G and Ci X. Nrf2 signaling and autophagy are complementary in protecting lipopolysaccharide/d-galactosamine-induced acute liver injury by licochalcone A. Cell Death Dis 2019; 10: 313.
[22] Pinho-Ribeiro FA, Zarpelon AC, Fattori V, Manchope MF, Mizokami SS, Casagrande R and Verri WA Jr. Naringenin reduces inflammatory pain in mice. Neuropharmacology 2016; 105: 508-519.
[23] Wang Q, Wang F, Li X, Ma Z and Jiang D. Quercetin inhibits the amphiregulin/EGFR signaling-mediated renal tubular epithelial-mesenchymal transition and renal fibrosis in obstructive nephropathy. Phytother Res 2023; 37: 111-123.
[24] Li J, Zheng X and Qi J. Research progress on the therapeutic mechanisms of stigmasterol for multiple diseases. Molecules 2025; 30: 1874.
[25] Meng XM, Zhang Y, Huang XR, Ren GL, Li J and Lan HY. Treatment of renal fibrosis by rebalancing TGF-β/Smad signaling with the combination of asiatic acid and naringenin. Oncotarget 2015; 6: 36984-36997.
[26] Gauthier T, Yao C, Dowdy T, Jin W, Lim YJ, Patiño LC, Liu N, Ohlemacher SI, Bynum A, Kazmi R, Bewley CA, Mitrovic M, Martin D, Morell RJ, Eckhaus M, Larion M, Tussiwand R, O'Shea JJ and Chen W. TGF-β uncouples glycolysis and inflammation in macrophages and controls survival during sepsis. Sci Signal 2023; 16: eade0385.

[27] Hou W, Lu L, Li X, Sun M, Zhu M and Miao C. c-Myc participates in high glucose-mediated endothelial inflammation via upregulation of IRAK1 expression in diabetic nephropathy. Cell Signal 2022; 92: 110263.
[28] Zhang H and Sun SC. NF-κB in inflammation and renal diseases. Cell Biosci 2015; 5: 63.
[29] Sue SC and Dyson HJ. Interaction of the IkappaBalpha C-terminal PEST sequence with NF-kappaB: insights into the inhibition of NF-kappaB DNA binding by IkappaBalpha. J Mol Biol 2009; 388: 824-38.
[30] Guo Q, Jin Y, Chen X, Ye X, Shen X, Lin M, Zeng C, Zhou T and Zhang J. NF-κB in biology and targeted therapy: new insights and translational implications. Signal Transduct Target Ther 2024; 9: 53.
[31] Wang M, Yang J, Fang X, Lin W and Yang Y. Membranous nephropathy: pathogenesis and treatments. MedComm (2020) 2024; 5: e614.
[32] Wang H, Lv D, Jiang S, Hou Q, Zhang L, Li S, Zhu X, Xu X, Wen J, Zeng C, Zhang M, Yang F, Chen Z, Zheng C, Li J, Zen K, Liu Z and Li L. Complement induces podocyte pyroptosis in membranous nephropathy by mediating mitochondrial dysfunction. Cell Death Dis 2022; 13: 281.
[33] Yi M, Zhang L, Liu Y, Livingston MJ, Chen JK, Nahman NS Jr, Liu F and Dong Z. Autophagy is activated to protect against podocyte injury in adriamycin-induced nephropathy. Am J Physiol Renal Physiol 2017; 313: F74-F84.
[34] Jung BK, Park Y, Yoon B, Bae JS, Han SW, Heo JE, Kim DE and Ryu KY. Reduced secretion of LCN2 (lipocalin 2) from reactive astrocytes through autophagic and proteasomal regulation alleviates inflammatory stress and neuronal damage. Autophagy 2023; 19: 2296-2317.
[35] Li H, Li P, Li S, Zhang X, Dong X, Yang M and Shen W. Mechanism of transforming growth factor-β1 induce renal fibrosis based on transcriptome sequencing analysis. Zhejiang Da Xue Xue Bao Yi Xue Ban 2023; 52: 594-604.
[36] Priyam J and Saxena U. Stage-specific coexpression network analysis of Myc in cohorts of renal cancer. Sci Rep 2023; 13: 11848.
[37] So BYF, Yap DYH and Chan TM. B cells in primary membranous nephropathy: escape from immune tolerance and implications for patient management. Int J Mol Sci 2021; 22: 13560.
[38] Moyo TK, Wilson CS, Moore DJ and Eischen CM. Myc enhances B-cell receptor signaling in precancerous B cells and confers resistance to Btk inhibition. Oncogene 2017; 36: 4653-4661.
[39] Deng B, Huang H, Deng L, Zhao Z, Liu M, Lin H, Wang X, Tian R, Tu X, Peng A, Liang E, Bao K, Zhou Y, Xu P and He M. Imbalance of T follicular helper cell subsets trigger the differentiation of pathogenic B cells in idiopathic membranous nephropathy. Inflamm Res 2024; 73: 485-498.
[40] Xu L, Tayier D, Yang S, Zhang X and Lu C. Follicular helper T cells and follicular regulatory t cells involved in immune disorders of idiopathic membranous nephropathy. Indian J Pediatr 2024; 91: 702-708.
[41] Chen JS, Chen A, Chang LC, Chang WS, Lee HS, Lin SH and Lin YF. Mouse model of membranous nephropathy induced by cationic bovine serum albumin: antigen dose-response relations and strain differences. Nephrol Dial Transplant 2004; 19: 2721-8.
[42] Ponticelli C and Glassock RJ. Glomerular diseases: membranous nephropathy--a modern view. Clin J Am Soc Nephrol 2014; 9: 609-616.
[43] Noor F, Asif M, Ashfaq UA, Qasim M, Tahir Ul and Qamar M. Machine learning for synergistic network pharmacology: a comprehensive overview. Brief Bioinform 2023; 24: bbad120.